

# Prediction and evaluation of abnormal formation pressure and fracture pressure in 'Maria' field, deep offshore, Niger delta

Ajibade A. M.<sup>1</sup>, Enikanselu P. A.<sup>2</sup>, Olowokere M. T.<sup>3\*</sup>

<sup>1</sup> Department of Physical Science, Ondo State University of Science and Technology, Okitipupa

<sup>2</sup> Department of Applied Geophysics, Federal University of Technology, Akure

<sup>3</sup> Department of Geology, Obafemi Awolowo University, Ile Ife

\*Corresponding author E-mail:

## Abstract

This work aimed at the establishment of pore pressure generation mechanisms and pore pressure prediction for the "Maria" Field, Niger Delta. The objectives are therefore to isolate the pressure behaviour of the reservoir of interest in the study area and build a robust geological pressure model; predict pore pressure; and identify overpressure zones from pressure/depth plots with supporting evidence from drilling and mud log data.

A velocity cube was built by geostatistically mapping the available well-log data in the area, constrained by depth horizons and a 3D trend. The velocity volume was calibrated with checkshot data from an offset well. The calibrated velocity-to-pressure transform was then applied to the trend-krigged velocities. To apply the pore-pressure transform, density at all locations were determined to calculate 3D volume of pressure.

Well log data from Four (4) wells within the study area were used to determine the compaction trend using shale acoustic parameters and depth, and to establish pressure mechanism and predict overpressure depth. Normal Compaction Trend (NCT) were drawn by fitting of trend lines to the interval velocity, porosity and density data as a function of depth below mudline. Pressure data in the form of repeat formation test (RFT), Leak of Test (LOT), and mud weight (MW) data were used in this study to calibrate the prediction.

The top of overpressure were determined in Maria-001, -014 and -015 as 3749.04 m (12300ft), 2727.96 m (8950ft) and 2712.72 m (8900ft) respectively. Maria-004 well revealed normal pressure trend from plotted pressure data. At shallow depths, the subsurface stratigraphy follows normal compaction trend (NCT) from well and seismic velocity models. However, the shifts from the NCT, as observed from resistivity, sonic velocity and porosity, indicated under-compaction of sediments as the cause of the abnormal pressure in the field. The predicted pore pressures were compared with offset well data and good match were observed. The results of this study lead to an understanding of the subsurface pressure distribution. There is velocity reversal with density increase as in Maria-001, 014 and 015 wells this is most likely indicative of undercompaction as the cause of the abnormal pressure. In Maria-001 where the velocity decreases with constant density values, secondary pressure is likely to be the cause of the abnormal pressure. Overpressure mechanism analysis using velocity-density cross-plot techniques showed that the plots have negative trends in three wells namely Maria-001, -004, and -014. Velocity reduction were observed in the three wells which suggests that Disequilibrium compaction was the only primary mechanism that created overpressure. Lateral transfer along faults and connected reservoir systems also could have contributed to overpressure generated from deep processes as shown in Maria-004.

**Keywords:** Use about five key words or phrases in alphabetical order, Separated by Semicolon.

## 1. Introduction

Knowledge of the pore pressure in the various zones is critical in terms of controlling the process while drilling a well. Bottom-hole pressure deviating from the expected, or normal, pressure gradients may cause various problems and instabilities. Kicks and loss of control of the well are the most critical problems that may occur and can lead to a blowout or loss of the section if not handled properly. Even when the problems are properly handled, such events still require valuable time for restoring the situation back to normal, thus increasing the cost of drilling. Ideally, maintaining a real-time knowledge of the formation pressure may minimize the occurrence of some of the events, making drilling more efficient. Such knowledge may serve as an early kick-warning tool and will lead to avoidance or minimized occurrence of kick incidents. The efficiency of most well control actions rely on applying the proper measures as quickly as possible after the initiation of the event.

### 1.1. Previous works

Bruno et al., (2011) applied porosity as a tool for overpressure detection and is demonstrated using plots of porosity versus depth for two wells in an X-field in the Niger Delta. The results of well-1 showed that initially high porosity values ranging between 25% and 35%,

(between 3000-5000ft) interpreted to be within the Benin Formation begin to decrease at a depth of 5000ft, this continues steadily to a depth of about 7000ft. However, after 7000ft depth, there is an abrupt shift of porosity values to the right. This point is considered to be the top of a geopressure zone. The high porosity value remains almost constant till a depth of 11,000ft., indicative of an overpressure zone.

Olatunbosun et al., (2014) investigated overpressure condition in Afam field using a suite of borehole logs and 3D seismic data with a view to detecting and predicting abnormal pressure zones in the area. The methodology employed knowledge of well lithology and more detailed information extracted from inverted seismic traces. The interval velocity data of some shot lines within the study field and its immediate environment were computed to ascertain the pressure variations and the geological model of the less known areas from seismic data. The results obtained revealed five tops of overpressure (TOV) at different depths as derived from seismic and lithologic logs including their lateral variations. Normal Compaction Trend versus velocities plots obtained from sonic logs also confirmed the identified overpressure zones. Furthermore, four hydrocarbon-bearing zones, which were overlain by thin over pressured shale beds, were delineated.

## 1.2. Aim and objectives of the study

This work aimed at the establishment of pore pressure generation mechanisms of the drilling window and to examine how pressure data could be used for quantification of exploration risk of future prospects for example, analysis of the risk for seal failure.

To meet this aim the objectives are as to: isolate the pressure behaviour of the reservoir of interest in the study area and build a robust geological pressure mode; predict pore pressure using density and sonic logs by the equivalent depth method and identify overpressure zones from pressure/depth plots with supporting evidence from drilling and mud log data.

## 1.3. Location of the study area

The study area is located within longitude 6.00°E and 6.30°E and latitude 4.5°N and 5.00°N. "Maria" Field is within the Coastal Swamp Depo belt (Fig. 1).

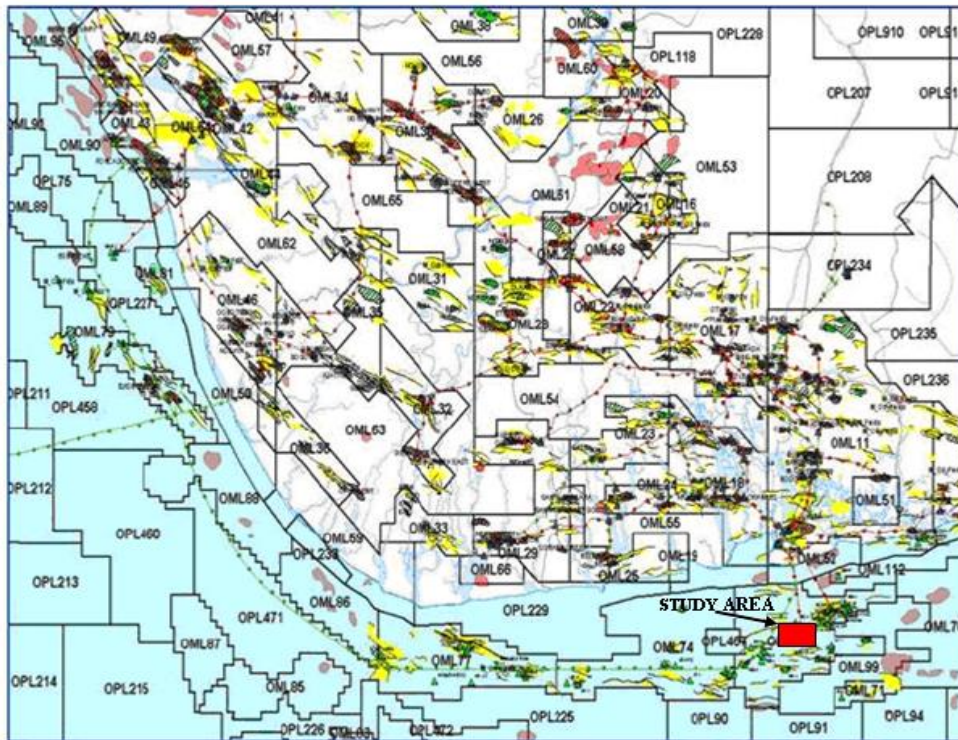


**Fig. 1:** Prospectivity Map of the Niger Delta Basin Showing the Different Oil Mining Leases (OML) and the Study Area.

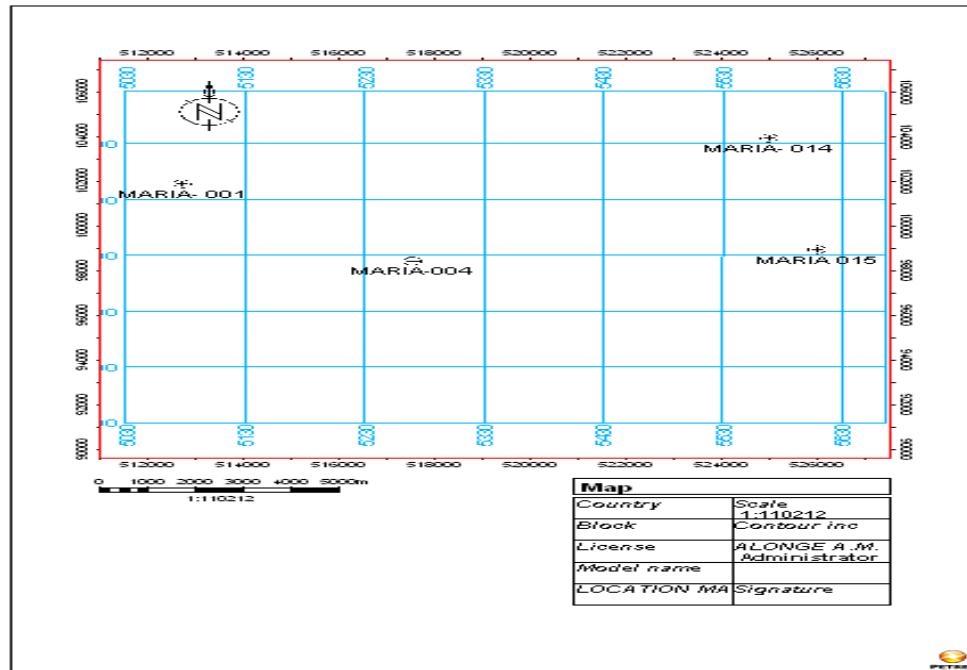


Fig. 2: Base Map of the Study Area Showing Inline, Crossline and Well Locations

## 2. Geology of Niger delta

### 2.1. Geological setting

The evolution of the delta is controlled by pre- and synsedimentary tectonics as described by Evamy et al. (1978), Ejedawe (1981), Knox & Omatsola (1987) and Stacher (1995). The delta growth is summarised below. The shape of the Cretaceous coastline (Fig. 3) gradually changed with the growth of the Niger Delta (Figs 4). A bulge developed due to delta growth. This changing coastline interacted with the palaeo-circulation pattern and controlled the extent of incursions of the sea (Reijers et al., 1997). Other factors that controlled the growth of the delta are climatic variations and the proximity and nature of sediment source areas.

During the Middle-Late Eocene, sediment was deposited (Fig. 3) west of the inverted Cretaceous Abakaliki High and south of the Anambra Basin in what became the 'northern depobelt of the Niger Delta' (Fig. 3). The first coarse clastic deposits have been dated on the basis of microfloral units (Evamy et al., 1978) as Early Eocene. Tradewinds generated longshore currents with two cells converging along the western estuarine coast sector (Burke, 1972; Berggren & Hollister, 1974; Reijers et al., 1997). Studies by Weber & Daukuro (1975), Ejedawe (1981) and Ejedawe et al. (1984) clarified that the embryonic delta subsided during the Late Eocene to Middle Oligocene <700 m/Ma and prograded approx. 2 km/Ma along three depositional axes that fed irregular, early delta lobes (Fig. 4) that eventually coalesced. Thick sandy sediment accumulations thus formed in the active 'Greater Ughelli depobelt'.

During the Late Oligocene to Middle Miocene, the delta subsidence remained steady at some 700 m/Ma but delta progradation increased to 8–15 km/Ma. Incision of the Opuama Channel (Figs 4a, 4b) in the western sector of the delta occurred at this time (Patters, 1984; Knox & Omatsola, 1987). From the Middle Miocene onward, the delta prograded over a landward dipping oceanic lithosphere. The 'Escalator Regression Model' of Knox & Omatsola (1987) shows the average delta subsidence rates and progradation figures used here. During the Miocene, the average progradation was some 1000 m/Ma. Depocentres in the eastern sector of the delta merged laterally and the enlarged delta front prograded pulse-wise, occasionally advancing at rates of 16–22 km/Ma (Figs 4a.). The coastline, now convex, broke up the longshore current into two divergent drift cells. During the Middle-Late Miocene, a rising hinterland supplied substantial amounts of sediment that accumulated in the active Central Swamp and in the northern sector of the Coastal Swamp. Progradation maintained at a steady rate of 13–17 km/Ma (Fig. 4a and b.) and stabilised in the Late Miocene-Pliocene when the Coastal Swamp and offshore depobelts became active. In the eastern delta, sedimentation was interrupted by cutting-and-filling events (Burke, 1972; Petters, 1984), resulting in the Agbada, Elekelewu, Soku and Afam 'channels' (Figs 4a and b.)

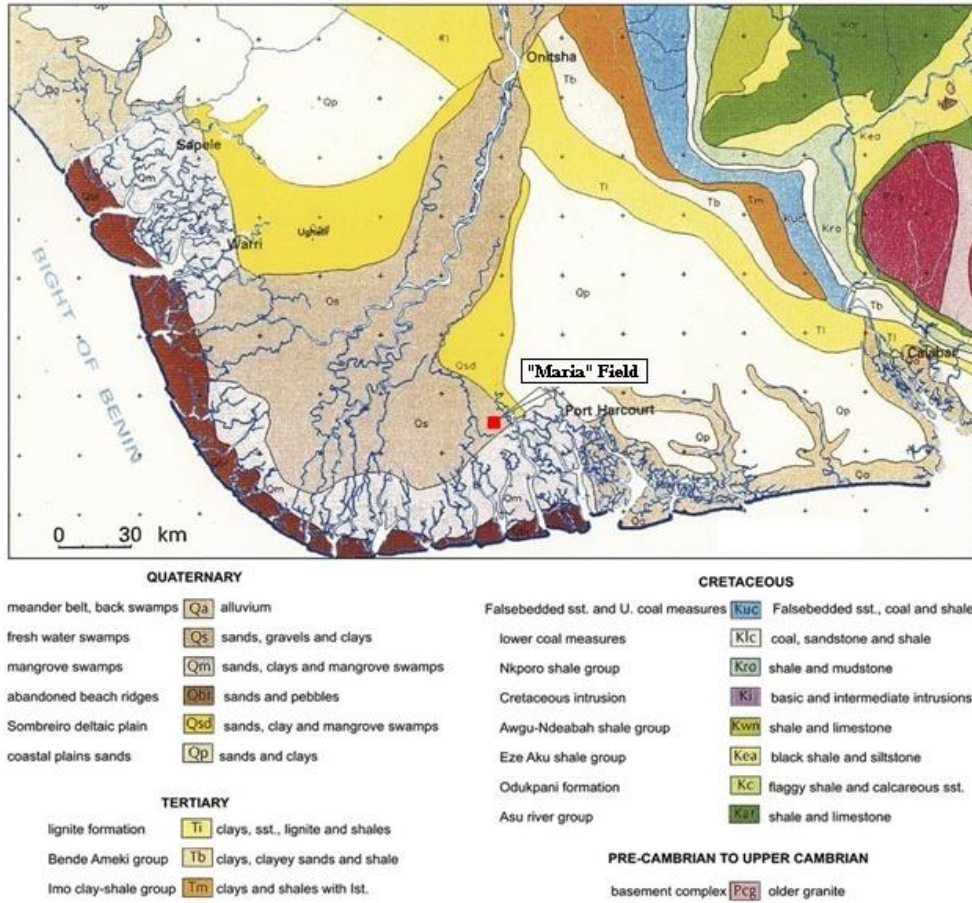


Fig. 3: Geological Map of the Niger Delta And Surroundings Showing Location of the Study Area.

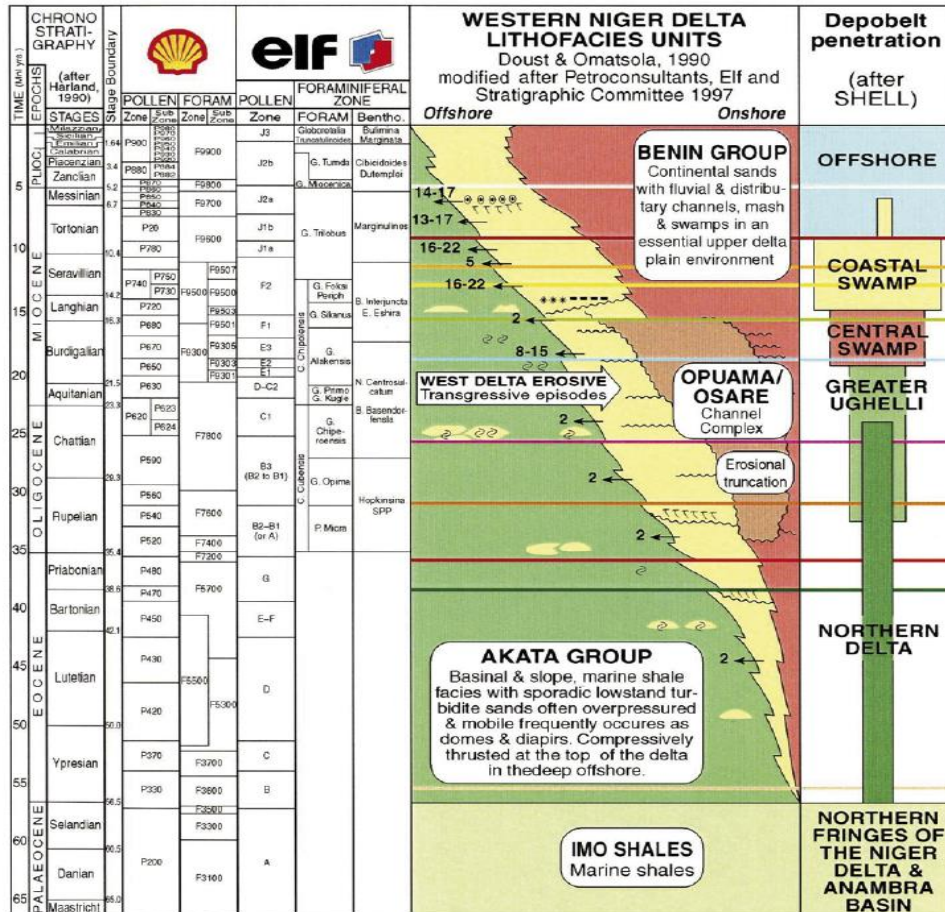


Fig. 4 A: Stratigraphic Data Sheet (West Half) of the Niger Delta.

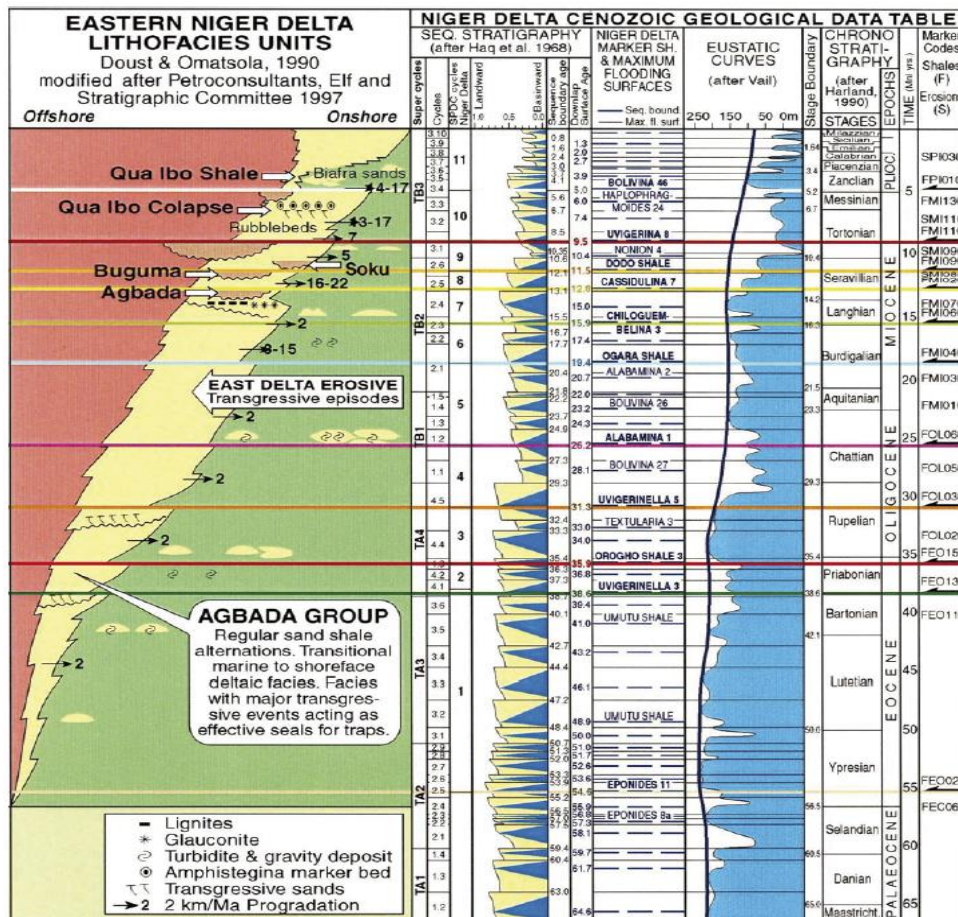


Fig. 4B: Stratigraphic Data Sheet (East Half) of the Niger Delta.

2.2. Structures

Most known traps in Niger Delta fields are structural although stratigraphic traps are not uncommon. The structural traps developed during synsedimentary deformation of the Agbadaparalic sequence (Evamy et al, 1978; Stacher, 1995). As discussed earlier, structural complexity increases from the north (earlier formed depobelts) to the south (later formed depobelts) in response to increasing instability of the under-compacted, overpressured shale. Doust and Omatsola (1990) describe a variety of structural trapping elements, including those associated with simple rollover structures, clay filled channels, structures with multiple growth faults, structures with antithetic faults, and collapsed crest structures (Fig. 5). On the flanks of the delta, stratigraphic traps are likely as important as structural traps (Beka and Oti, 1995). In this region, pockets of sandstone occur between diapiric structures. Towards the delta toe (base of distal slope), this alternating sequence of sandstone and shale gradually grades to essentially sandstone.

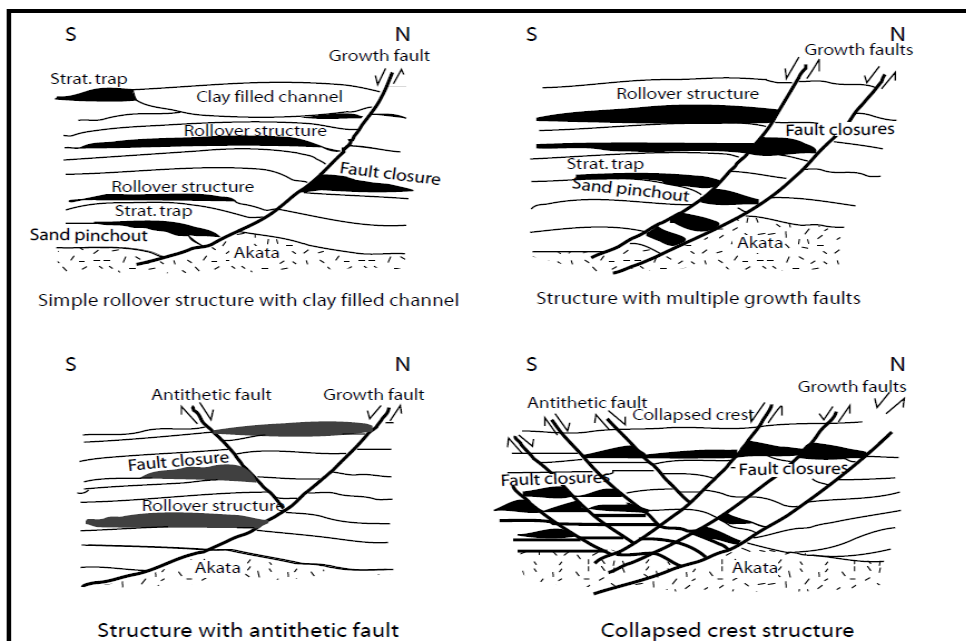


Fig. 5: Examples of Niger Delta Oil Field Structures and Associated Trap Types. Modified from Doust and Omatsola (1990) and Stacher (1995).

### 3. Materials and method of data analysis

#### 3.1. Data set and data presentation

Seismic interval velocity extracted from RMS velocity from 3D seismic data volume within the study area was used for this study. Data from a total of 4 wells: petrophysical logs, wireline test data were compiled for each well. Drilling data was available for PP prediction, measurements and calibration. Measurement While Drilling (MWD), conventional logs, (sonic logs, gamma ray and density logs) mud log, direct Pore Pressure measurements in the sand (Repeat Formation Test (RFT), and Mudweight) and engineering drilling records were used to establish the subsurface geopressure profile.

#### 3.2. Method of data analysis

Methods used to determine the formation pressure can be divided into two categories: prediction methods and detection methods. Prediction methods are based on seismic velocities data and offset well logs (Bourgoyne et al., 1991). Pore pressure detection methods use drilling parameters and well logs, logging while drilling data (LWD) (Bourgoyne et al., 1991).

#### 3.3. Pore pressure prediction model from seismic velocity

The pore pressure model was built along the 3D structural grid, using the empirical relationship between pore pressure and velocity. Pore pressure data is treated as a property, upscaled and distributed along the 3D structural grid based on interval velocity from the sonic (distributed with a geostatistical approach). The existing 3D geological model, complete with structural framework, reservoir zonation, and petrophysical analysis were utilized to model the anticipated abnormal pressure.

The velocity model, thus obtained, went through geostatistical mapping using the upscaled well log velocities within some key stratigraphic layers.

The velocity-to-pore-pressure transform was derived from data from wells in the area of interest or offset wells. Fitting of trend lines to velocity data as a function of depth below mudline was done. This trend is often referred to as a "normal trend" which captures the expected velocity variation with depth when the pore pressure is hydrostatic. The calibration of the transform is based on evaluating the misfit between the predicted pore pressure and the measured pore pressure and is quantified by the root mean square (rms) of the residuals (Sayers et al., 2002). An estimate of the inherent uncertainty is given by minimizing and mapping the rms with respect to the parameters that define the pore-pressure transform.

Pore-pressure data used for calibration were obtained from an analysis of mud weights and formation pressure test data. The calibrated velocity-to-pressure transform was then applied to the trend-krigged velocities. To apply the pore-pressure transform, density at all locations were determined to calculate 3D volume of pressure. A velocity cube was built by geostatistically mapping the available well-log data in the area, constrained by depth horizons and a 3D trend. The use of horizons helped to maintain consistency of the well data and the geologic structure. The velocity-to-pore-pressure transform, which is established from nearby well data, is then applied to this trend-krigged velocity volume.

#### 3.4. Determination of normal compaction trend

An example of an estimated NCT in the study area is shown in Figure 6. Because the NCT is a required input for pressure prediction using the equivalent depth method and Eaton's method, it must be as accurate as possible. The major challenges in constructing NCTs for wells in this study are estimation of the trend in the shallow sections of wells where density logs are not available and onset of overpressure in the shallow section of a well, making it difficult to establish the NCT even in the shallow section. Normal Compaction Trend (NCT) is drawn from the variation interval velocity with depth for four wells

#### 3.5. Determination of overburden gradient and pore pressure gradient

Pressure gradient were calculated in reservoirs using wire-line tools like Repeat Formation Tester (RFT) and the Modular Dynamic Tester (MDT) which are the measured pressure in permeable beds at specific depth. The pressure-depth data were plotted on linear graph sheets. Gradient of the trend line were determined between two depth points within each compartment.

Pressure gradient in the reservoirs was calculated referencing with reference to the subsea level (SL) so as not to cause serious mistake in the reservoir formation's fluids gradient.

Shale pressure gradients were determined using exponential trend (power-law forms) in the geo pressured zone because seal pressure gradient follow power law.

In order to overcome the mismatch between the measured and predicted pressure values, the Normal Compaction Trend for the study area was broken into many segments. In this study, Eaton's Method was applied.

All the four wells viz. Maria-001, Maria-004, Maria-014, Maria-015 locating at the Study area are served as deepwater - exploratory wells. The four wells have been drilled up to 9063 m, 86663.5 m, 7188 m, and 7546 m. Pore Pressure Gradient of each well has been estimated separately by using Miller's Sonic Equation. Overburden Gradient (OBG) has been calculated using bulk density equation. OBG and PPG have been studied for selected depth interval of 4462-9063ft, 6605-8663ft, 6540-7188ft and 6890-7546ft for the four wells.

## 4. Results and discussion

Iso-velocity layer overlaid on the seismic section shows the various velocity field in the lateral and vertical direction. It shows that velocity reversal occurred at shallow depth (within the vicinity of Maria-014). Normally velocity has to increase with depth. Figure 7 shows overlay of seismic velocities with reflectivity data near Pre-Stack Depth Migrated (PSDM) data: Crossline 1707 and Inline 5260.

In this study we use a layer-based tomography, where the subsurface is described by a network of interlocking closed bodies best thought of as polygons rather than layers. Within each polygon the velocity is represented by a laterally continuous function, while velocity changes discontinuously across the polygon interface. Polygon velocities and thicknesses are updated in successive tomographic itera-

tions. The objective is to find both the interface locations and the lateral velocity function within each polygon, which yields the flattest reflections in prestack migrated gathers (Kosloff et al., 1996). Layer-based tomography makes use of the structural framework as a constraint for interpolating velocity from one analysis point to the other. In the present situation, where velocities vary much less within the layers than between them, this framework is an effective constraint on interpolation. The equations relating the time errors to changes in the model are solved by a weighted least-squares technique.

Seismic Velocity Volume of the study area was extracted using seismic interval velocity from prestacked depth migrated data (Figure 9). Figure 11 show the results of the velocity-pressure transform i.e. pore pressure prediction Model. Calibrated Interval velocity volume was converted from time domain to depth domain using the checkshot data for pore pressure prediction. Zone of velocity reversal are shown with the dashed circles. Vertical variation of velocity is observed within the vicinity of Maria -014 on arbitrary seismic lines, one of which crosses the well.

Pore pressure varies from 50 psi to 4000 psi with observed high pressure that varies from 2800 to 3200 psi observed around well Maria-004 and Maria-014, while slightly higher pore pressure (3250 psi to 3600 psi) is predicted in well Maria-001 and Maria-014 (Figs. 9 and 11). The results in Figure 6 support the hypothesis that the four wells are drilled in three isolated pressure compartments. Although the pressures in wells Maria-014 and 015 are similar, the apparent high-velocity zone between those wells may indicate the existence of an isolated compartment with lower pressure (Fig. 12.)

Seismic line 5600 reveals zone with abnormal pressure gradient well above 0.65psi/ft around Maria-014 (Fig. 11). A normal pressure gradient in the Niger Delta is in the range of 0.442psi/ft. The abnormal pressure could be as a result of fluid migration through the fault shown on the section. The Depth map in Fig. 10 showed presence of faults at the E4.2 depth. The Horizon experienced structural discontinuity. The reflection continuity is low to moderate because the depth is close to the top of Akata Formation.

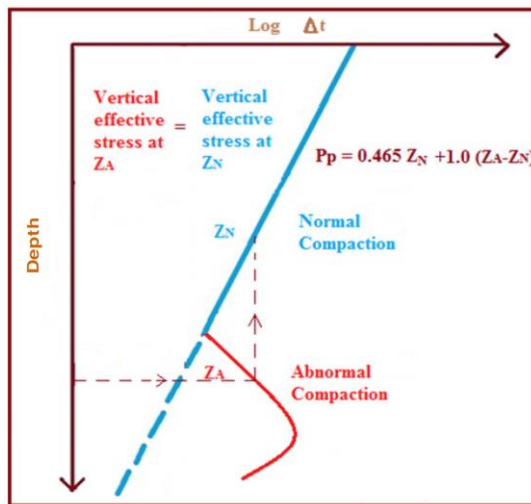


Fig. 6 A: Normal Compaction Trend from Equivalent depth method

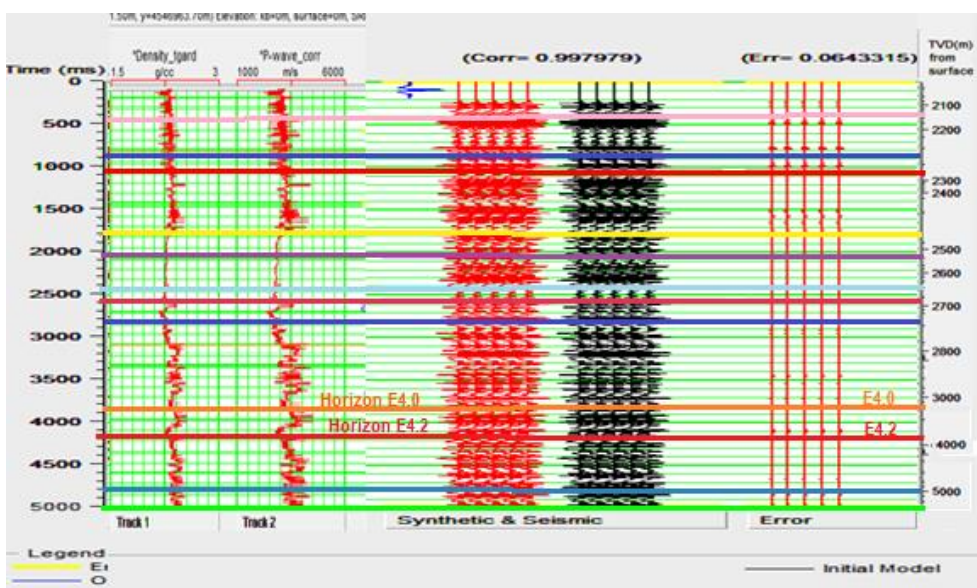


Fig. 7 A: Well Log, Synthetic Seismogram and Surface Seismic Correlation for Well Maria-014 and Inline 1707.

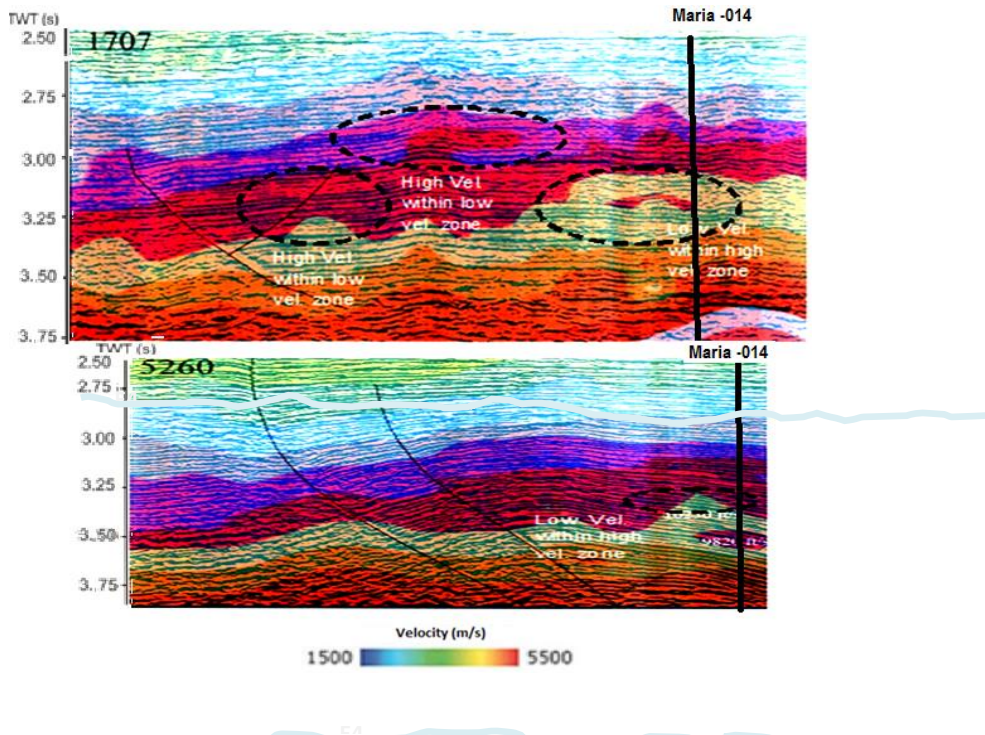


Fig. 7 B: Overlay of Seismic Velocities with Reflectivity Data Near Stack Pre-Stack Depth Migrated (PSDM) Data: Crossline 1707 and Inline 5260.

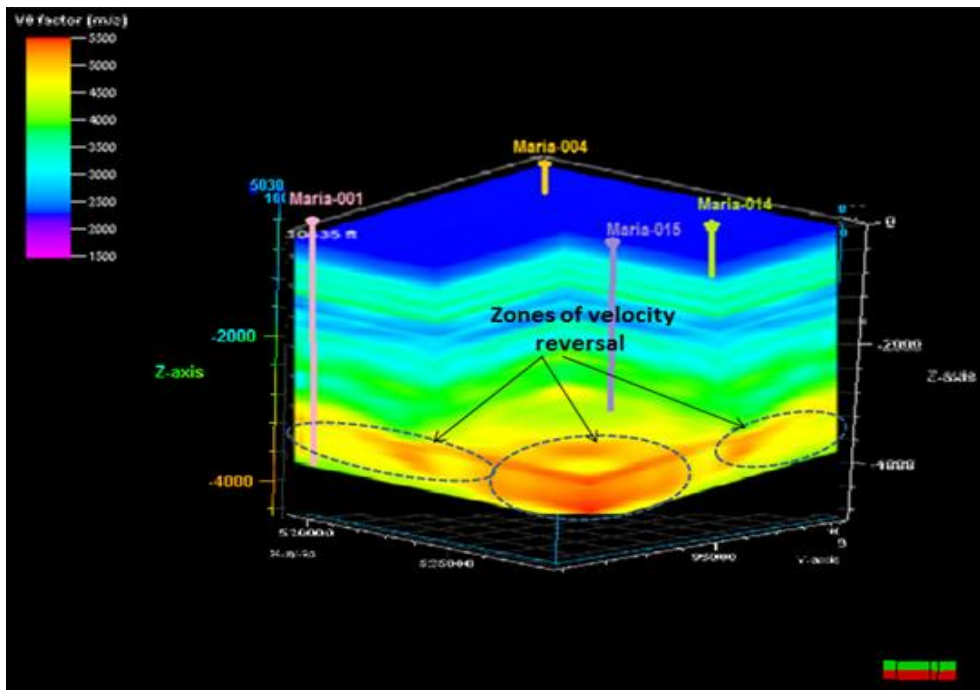


Fig. 8: Seismic Velocity Model Used for Pore Pressure Prediction.

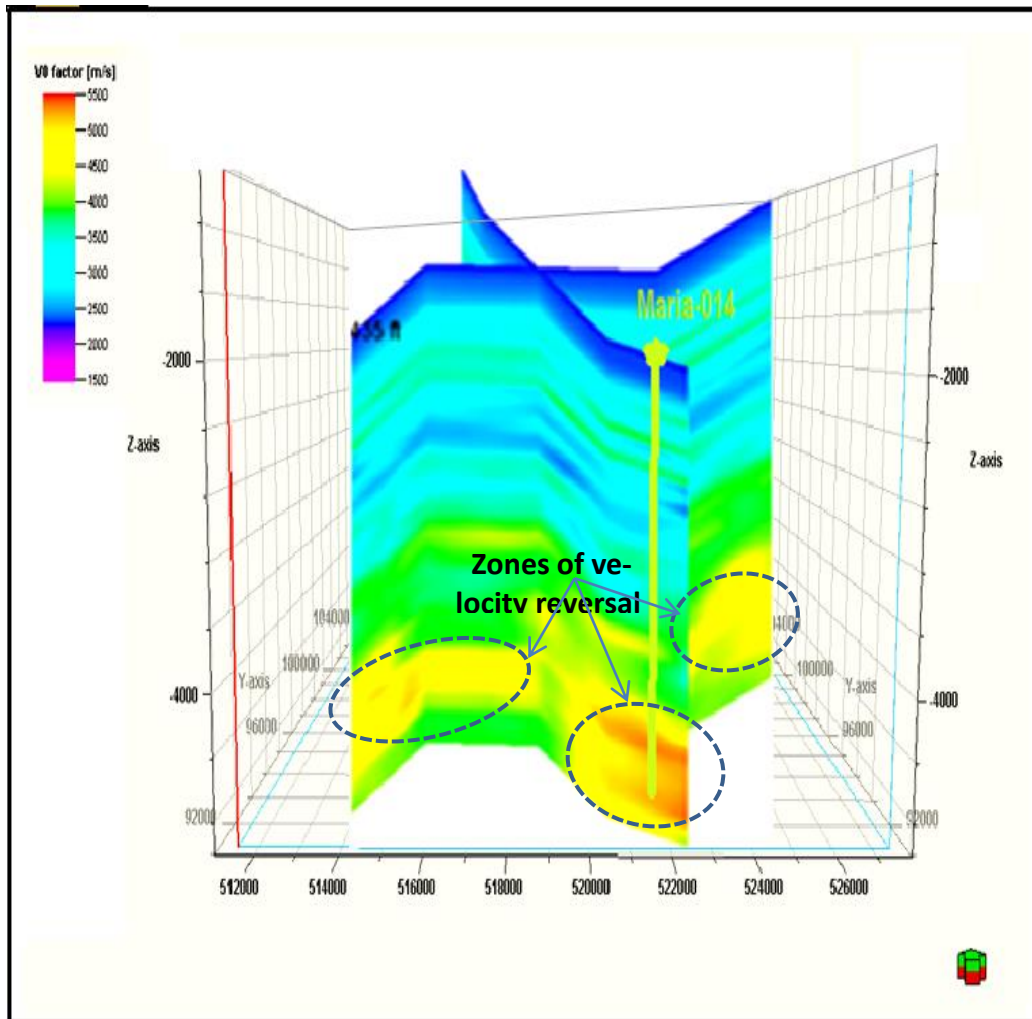


Fig. 9: Velocity Model in Two Arbitrary Lines Used for the Pressure Prediction.

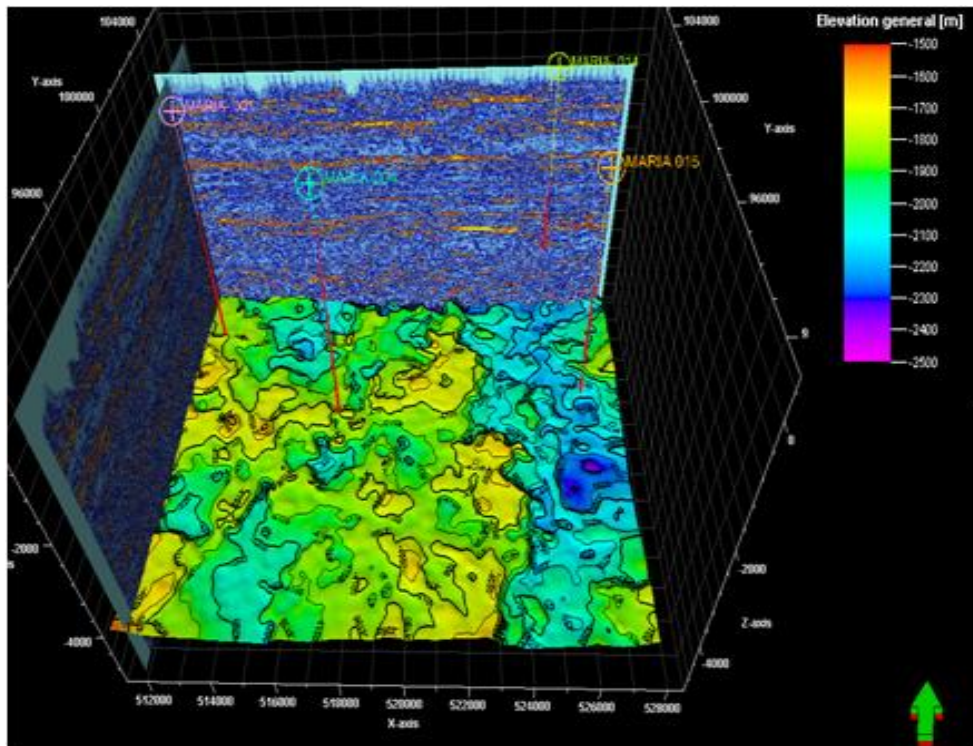


Fig. 10: Depth Structure Map of Horizon E4.2 (Top of the Geopressure Shale).

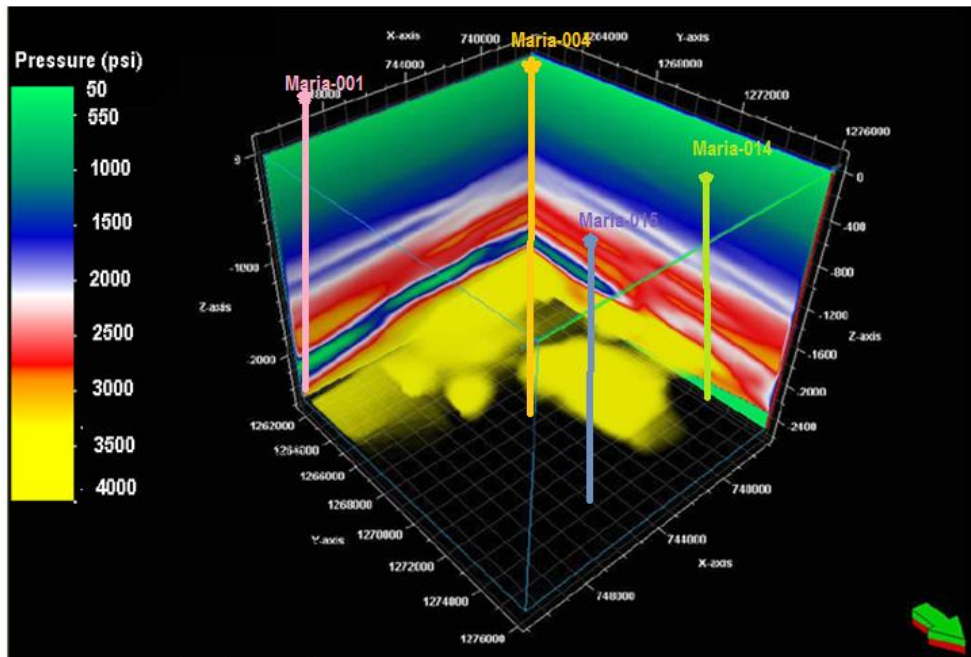


Fig. 11: 3D Volumes of Geopressure Model in Depth Domain Showing the Inline, Cross Line and Time Slice at Z=2400m.

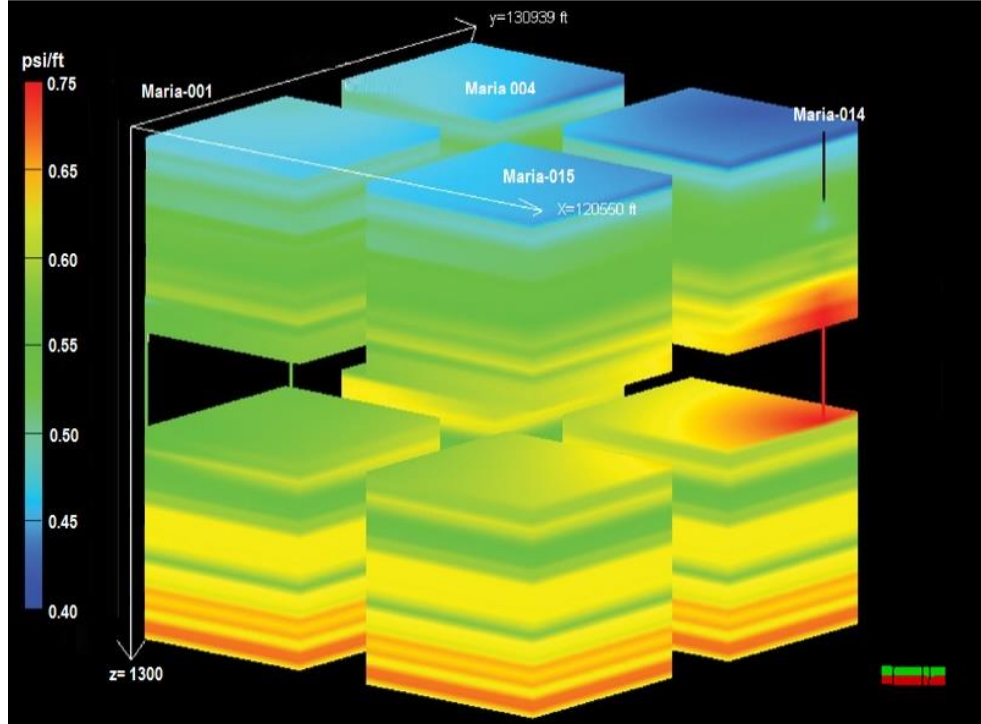


Fig. 12 A: Extraction of Pore Pressure Cubes Around Available Well Locations.

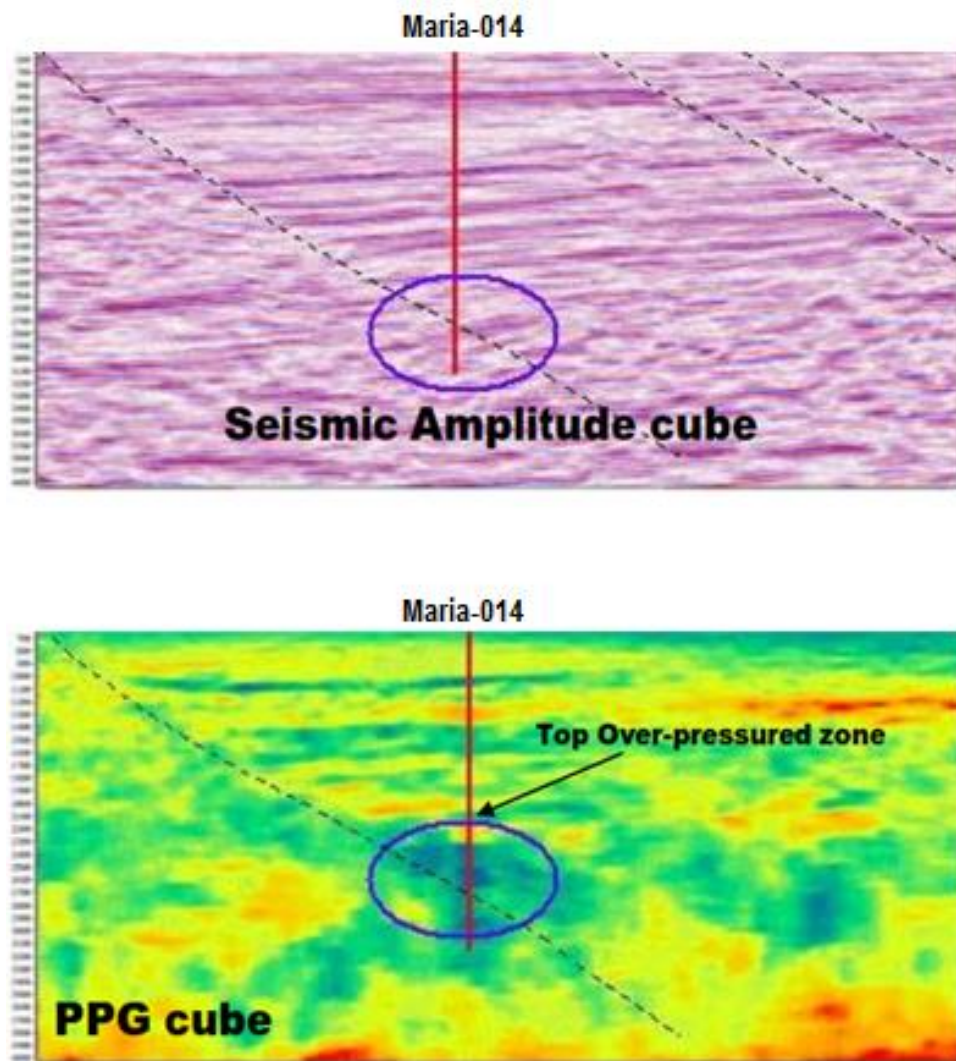
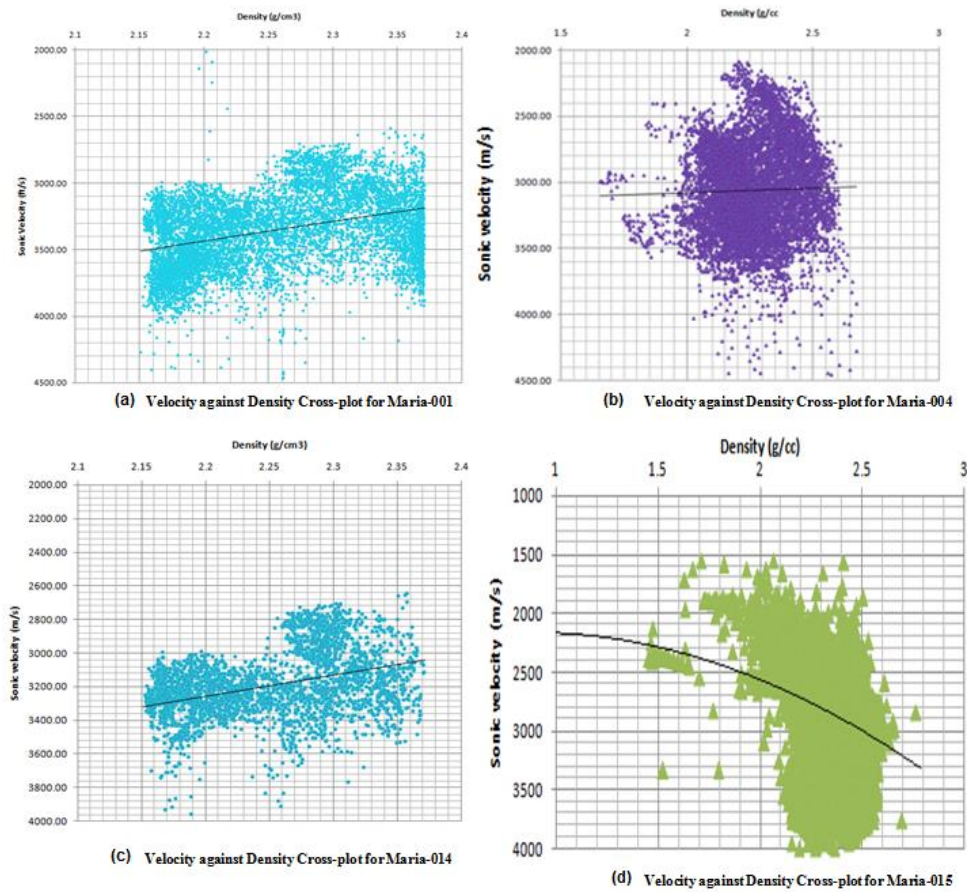


Fig. 12 B: Extraction of Pore Pressure on Inline 5600 Around A Well Location

## 5. Pressure mechanism from velocity versus density cross plot

This study inferred that disequilibrium compaction is the primary source of overpressure generation in the study area, caused by high sedimentation rates. Using traditional technique of pore pressure prediction of Eaton (1975) gives inadequate result from comparison with control pressure data. New relationships was developed based on integrating an understanding of basin history, shale behaviour, clay mineral diagenesis, thermal behaviour and geological time which successfully predict pore pressures in this area.

The density and sonic data of the formation showing in Figure 13 and Figure 15 for Maria- 004 and Maria-015 respectively give a good indication of the maximum compaction achieved by the rocks. Whereas there is velocity reversal with density increase as shown in Figure 12 and Figure 14 for Maria-001 and 014 respectively, this is most likely indicative of undercompaction as the cause of the abnormal pressure. In Maria-001 where the velocity decreases with constant density values, secondary pressure is likely to be the cause of the abnormal pressure. Overpressure mechanism analysis using velocity-density cross-plot techniques showed that the plots have negative trends in three wells namely Maria-001, -004, and -014. Velocity reduction were observed in the three wells which suggests that Disequilibrium compaction was the only primary mechanism that created overpressure. Lateral transfer along faults and connected reservoir systems also could have contributed to overpressure generated from deep processes as shown in Maria-004.



**Fig. 13:** Velocity-Density Plots for All the Wells.

Figure 14 to 17 showed the pore pressure profile of gamma-ray, density, sonic velocity and Porosity plot for Maria-001, Maria-004, Maria-014, and Maria-015, plotted individually. The idea is to check whether reversals have occurred at the same depth in all of the log types, or just in some.

The Normal Compaction Trend (NCT) relied on several aspects. Stratigraphy and frequency of seals to reservoirs determine the slope and extent of NCT. The study showed that structural high are associated with higher NCT slope (higher PG) and, conversely, structural low showed low NCT slope (lower PG). This is because structural setting has an immense impact on the slope and extent of the NCT slope. Moreover, because the structural setting of a lead or a prospect has a direct impact on the NCT's slope, there are different NCT for the area of study.

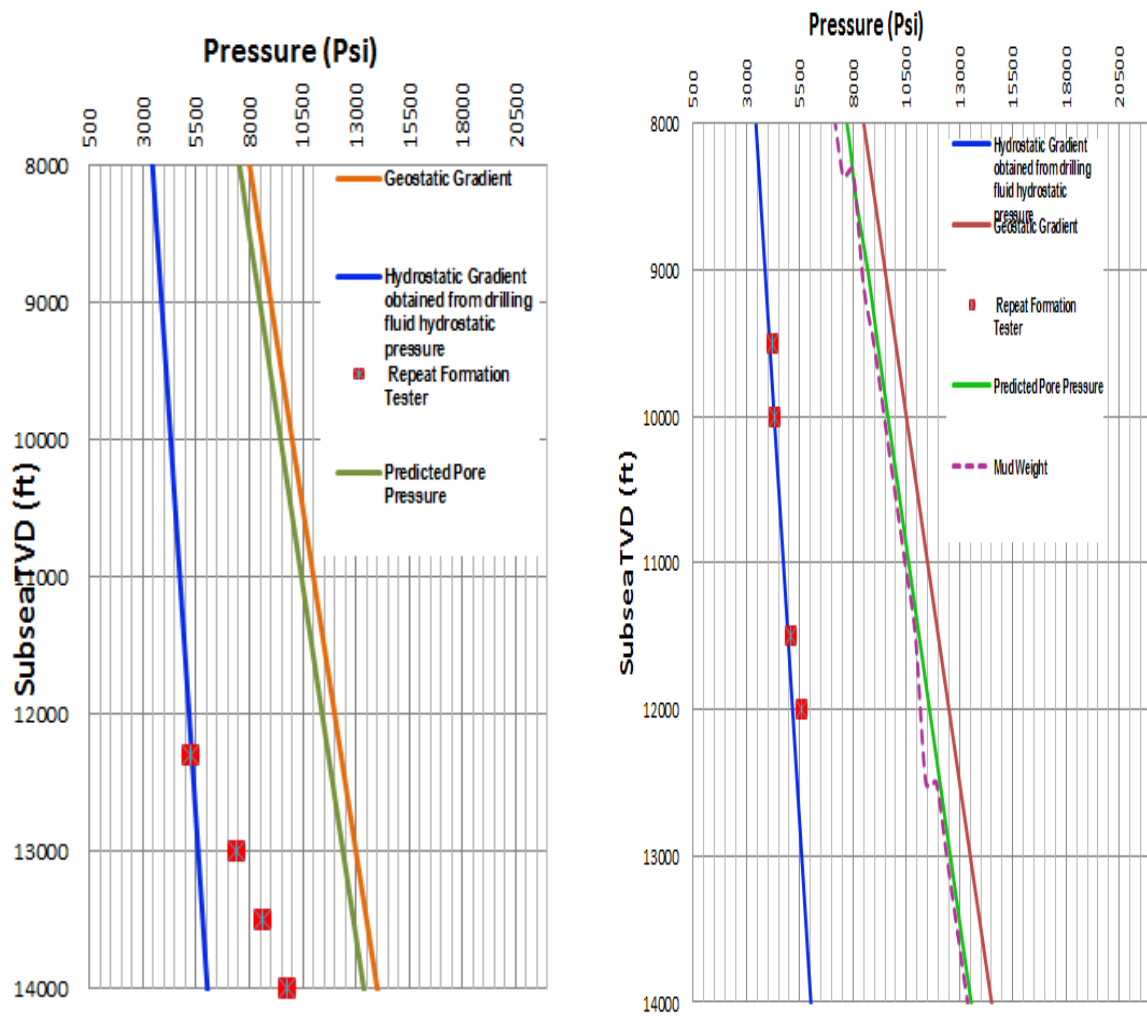


Fig. 14: Pressure (Psi) -Depth Plot of Maria-001 and Maria 004. From repeat Formation Test Data of the Study Area

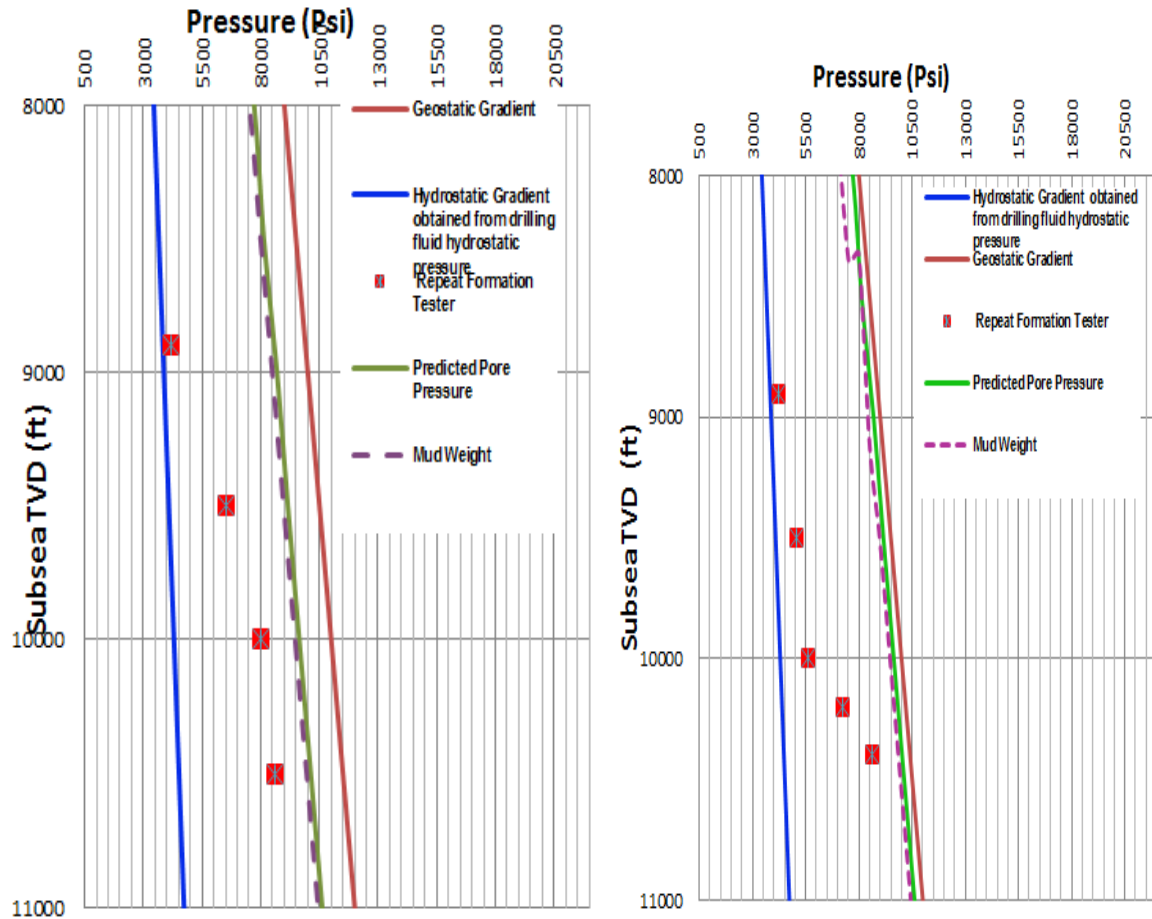


Fig. 15: Pressure (Psi) -Depth Plot of Maria-014 and Maria 015. From repeat Formation Test Data of the Study Area

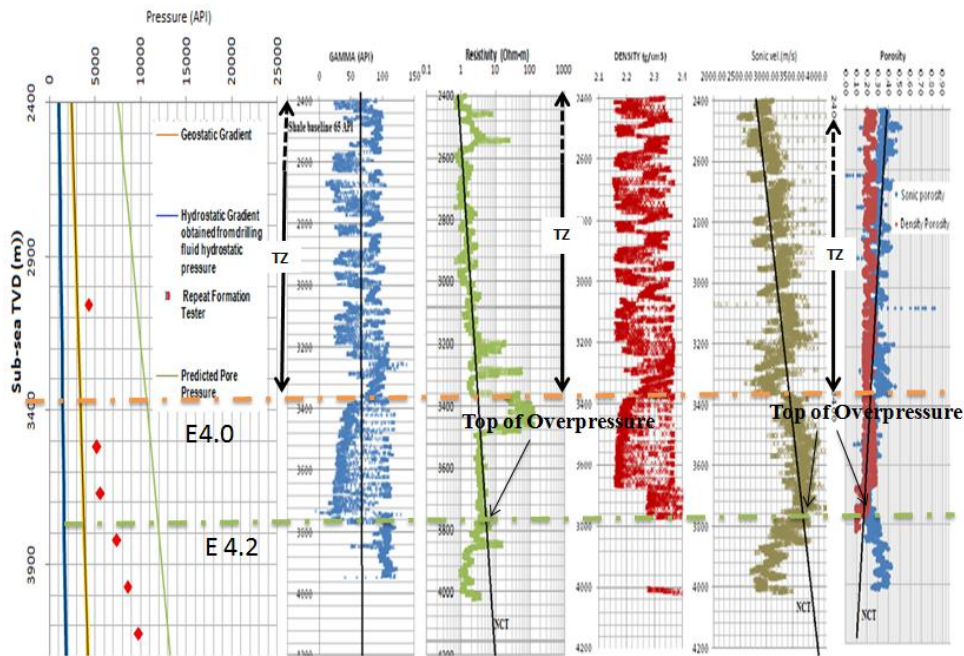


Fig. 16: Plots of Pressure, Gamma-Ray, Resistivity, Density, Sonic Velocity and Density/Sonic Porosity for Well Maria-001.(2438.4-3962.4 M Depth).

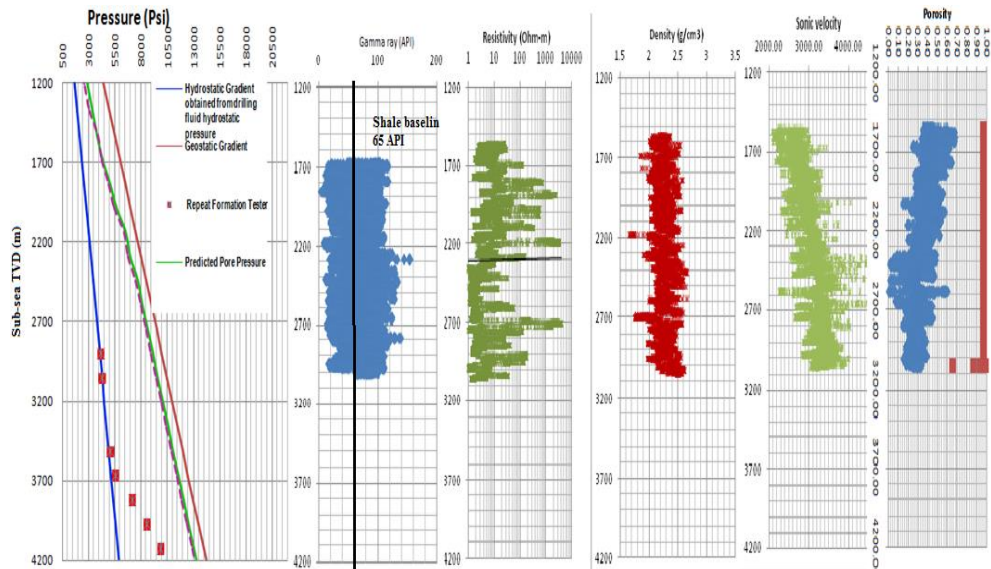


Fig. 17: Plots of Pressure, Gamma-Ray, Resistivity, Density, Sonic Velocity and Density/Sonic Porosity for Well Maria-004. (1219.2-3048 M Depth).

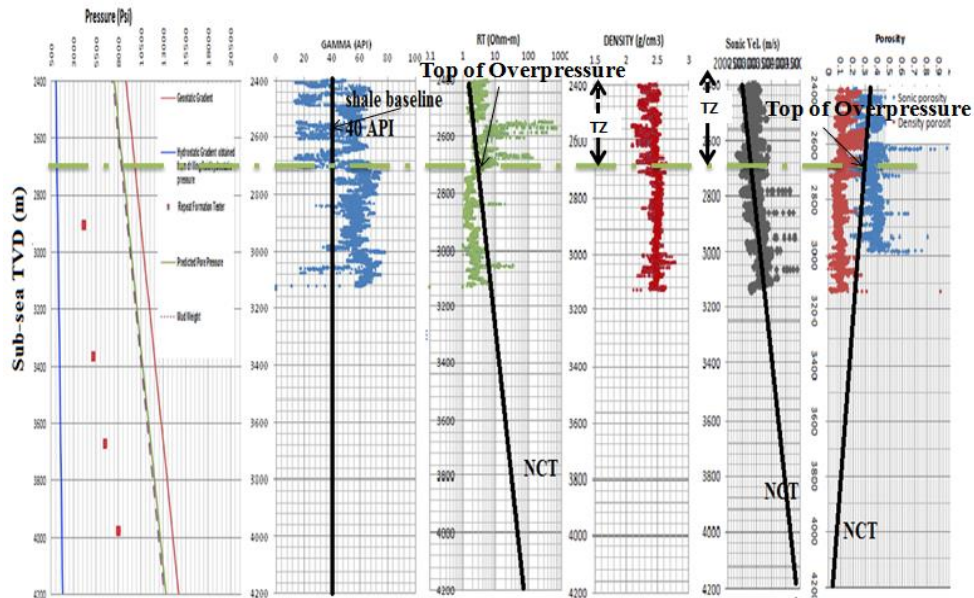


Fig. 18: Plots of Pressure, Gamma-Ray, Resistivity, Density, Sonic Velocity and Density/Sonic Porosity for Well Maria-014. (2438.4-3169.92 M Depth).

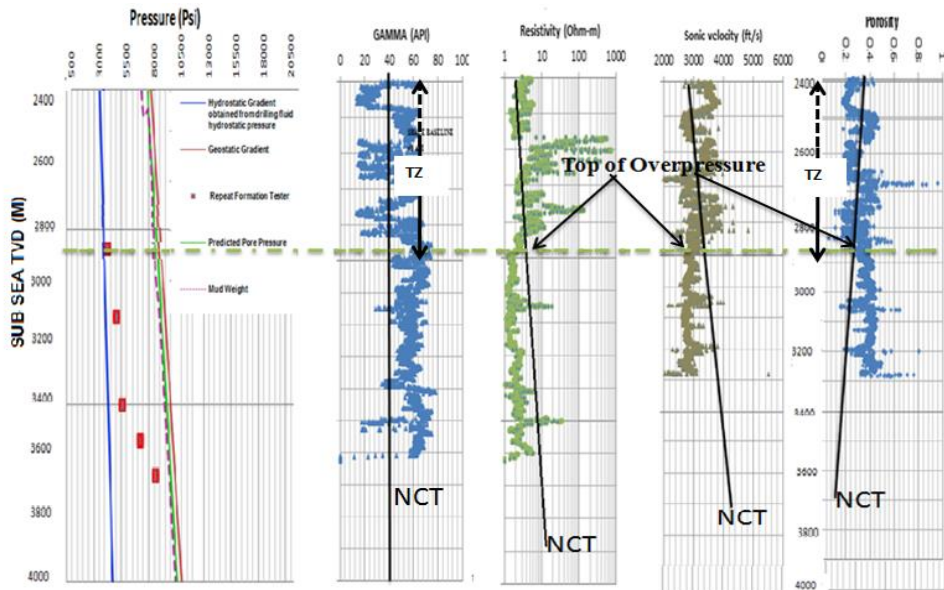


Fig. 19: Plots of Pressure, Gamma-Ray, Resistivity, Density, Sonic Velocity and Density/Sonic Porosity for Well Maria-015, (2438.4-3169.92 M Depth).

### 5.1. Interpretation of sealing capacity from NCT

Maria-0.14 Wells drilled on the crest and in proximity of a ridge show higher NCT slope gradient and consequently a higher PP gradient. This was the case where Transition Zone (TZ) covers a short interval of about 61 m (2000') and NCT shows high slope gradient (Fig. 19). Note the mud-weight profile shows a sharp increase crossing the Top of Overpressure (TOG) zone to the geopressured compartmentalization below.

Figures 18 and 19 showed the short extent and high slope of the NCT in the study area with Well Maria-014 and 015. This led to effective geopressure compartmentalization and consequently high sealing capacity.

Geopressure analysis was conducted on this well using resistivity to predict PP in the shale and the measured RFT's in sand beds. This analysis showed a possible weak TOG at 2880m (9417ft), as indicated in Figure 19. Meanwhile, the measured pressure in the sands between 2400 and 3400m shows a linear trend. The gradient of this trend is slightly higher than the regional Niger Delta with hydrostatic gradient (0.465 psi/ft) and it might represent a typical transition Zone (TZ) gradient. NCT has a very steep slope and thin TZ interval which exceeds 1000m. Pore pressure build up is very high and compartmentalization – sealing capacity is very good.

## 6. Conclusion

Velocity, density and resistivity increase in correspondence with the water expulsion rate in this zone. The Normal Compaction Trend (NCT) represents the optimum fitted linear trend of these measured data in the low permeable beds in TZ.

Subsurface stratigraphy and structural settings directly impact NCT slope and confinement. In this study area that occur on inner shelf, structural settings where coarse sediments dominate, NCT shows a gentle slope and a long Transition Zone (TZ)

Data acquisition, processing and quality affect NCT slope and PP prediction results. Therefore, choosing the adequate petrophysical measurements from seismic, well logs and check-shot surveys is essential for PP analysis. Well logs images in collaboration with digital images are very helpful in establishing NCT slope and extent.

Tampering and breaking the NCT into multiple segments for the purpose of calibrating the predicted PP can lead to serious pitfalls in pressure modeling results. Pore pressure prediction is a function of geological setting rather than data manipulation.

The fundamental aspect in 3D pore pressure distribution is an empirical relationship between the pore pressure and velocity. This relationship enables the pore pressure prediction to be distributed in 3D model that follow the trend of the velocity.

The results of this 3D pore pressure prediction model imaged the pressure profile of surrounding area with limited data and provide drilling engineers and operation geologists to reduce drilling hazard, in this case abnormal pressure from hydrocarbon or shale.

In conclusion, in the Maria Field, there is a strong correlation between rate of sedimentation and overpressure development by disequilibrium compaction. As wells go deeper into this formation (below the 100°C isotherm), thermal processing shales results in secondary overpressure generation, and, this overpressure is transmitted to reservoirs.

## References

- [1] Alixant, J.L. and Desbrandes, R. (1991): "Explicit Pore-Pressure Evaluation: Concept and Application," SPEDE p. 182. <https://doi.org/10.2118/19336-PA>.
- [2] Ajakaiye, D.E. & Bally, A.W. 2002a. Course manual and atlas of structural styles on reflection profiles from the Niger Delta. American Association of Petroleum Geologists, Continuing Education Course Note Series, 41. <https://doi.org/10.1306/CE41915>.
- [3] Bilotti, F. & Shaw, J.H. 2005. Deep-water Niger Delta fold and thrust belt modeled as a critical-taper wedge: The influence of elevated basal fluid pressure on structural styles. American Association of Petroleum Geologists Bulletin, 89, 1475–1491. <https://doi.org/10.1306/06130505002>.
- [4] Bilotti, F., Shaw, J.H., Cupich, R.M. & Lakings, R.M. 2005. Detachment fold, Niger Delta. In: Shaw, J.H., Connors, C. & Suppe, J. (eds) Seismic interpretation of contractional fault-related folds. American Association of Petroleum Geologists, Studies in Geology, 53, 103–104.
- [5] Briggs, S.E., Davies, R.J., Cartwright, J.A. & Morgan, R. 2006. Multiple detachment levels and their control on fold styles in the compressional domain of the deepwater west Niger Delta. Basin Research, 18, 435–450 <https://doi.org/10.1111/j.1365-2117.2006.00300.x>.
- [6] Bolas, H.M.N., Hermanrud, C and Teige, G.M.G.: 2004. Origin of overpressures in shales: constraints from basin modelling; AAPG Bulletin, vol.88, no.2; pp.193- 211. <https://doi.org/10.1306/10060302042>.
- [7] Bourgoyne, A.T. Jr, and Rocha, A.L. Jr. (1996):
- [8] Caillet, G., and S.Batiot.: 2003. 2-D modelling of hydrocarbon migration along and across Growth faults: An example from Nigeria: Petroleum Geoscience, vol.9; pp.113-124. <https://doi.org/10.1144/1354-079302-499>.
- [9] Carcione, J.M., and H.B. Helle, 2002, Rock physics of geopressure and prediction of abnormal pore fluid pressure using seismic data: CSEG Recorder, v. 27/7, p. 8-32.
- [10] Chopra, S, and A. Huffman, 2006, Velocity determination for pore pressure prediction: Leading Edge, v. 25/12, p. 1502-1515. <https://doi.org/10.1190/1.2405336>.
- [11] Clegg, P., 2011, Understanding Overpressure and its Prediction, Training Module: IPA.
- [12] Corredor, F.H., Shaw, J.H. & Bilotti, F. 2005a. Structural styles in the deep-water fold and thrust belts of the Niger Delta. American Association of Petroleum Geologists Bulletin, 89, 753–780. <https://doi.org/10.1306/02170504074>.
- [13] Corredor, F.H., Shaw, J.H. & Suppe, J. 2005b. Shear fault-bend fold, deep water Niger Delta. In: Shaw, J.H., Connors, C. & Suppe, J. (eds) Seismic interpretation of contractional fault-related folds. American Association of Petroleum Geologists, Studies in Geology, 53, 87–92.
- [14] Crain, E. R. (1986). The log analysis handbook. Tulsa, OK: Penn-Well.
- [15] Desbrandes, R. (1985). Encyclopedia of well logging. Houston, TX: Gulf.
- [16] Doust and Omatsola (1990).
- [17] Eaton, B.A. (1975): "The Equation for Geopressure Prediction from Well Logs," paper SPE 5544 presented at the 1975 SPE Annual Technical Conference and Exhibition, Dallas, TX, September 28 – October 1. <https://doi.org/10.2118/5544-MS>.
- [18] Hilchie, D. W. (1982). Advanced well logging interpretation. Golden, CO: D.W.
- [19] Hoesni, M.J., Swarbrick, R. E, and Gouly, N. R (2003). The Origins of overpressure in the Malay Basin AAPG Barcelona Conference, Spain.
- [20] Hottman, C.E., and Johnson, R.K.: "Estimation of Formation Pressures from Log-derived Shale Properties," JPT, June 1965, p. 717 <https://doi.org/10.2118/1110-PA>.
- [21] <http://www.onepetro.org/mslib/app/Preview.do?paperNumber=00005544&societyCode=SPE>
- [22] Indrelid, S.L., 1997. A guide to the prediction of pressures from seismic velocities; SIEP-97-5790.
- [23] Iverson et al., 1994.
- [24] Krusi, H.R., 1994. Overpressure prediction; A contribution towards safer drilling; Nigeria Association of Petroleum Explorationists Bulletin, vol.9; pp.86–91.
- [25] Krueger, S.W. & Grant, N.T. 2006. Evolution of fault-related folds in the contractional toe of the deepwater Niger Delta. Paper presented at the AAPG Annual Convention, 9–12 April, Houston, Texas. Search and Discovery, article #40201, available on the World Wide Web at <http://www.searchanddiscovery.net/documents/2006/06060krueger/index.htm>.

- [26] Krueger, S.W., Snyder, F.C., Grant, N.T., Beeley, H.S., Maler, M., Parry, C.C. & Solomon, S. 2005. Evolution of fault-related folds in the contractional toe of the deepwater Niger Delta (abstract). In: Proceedings of the International Conference on Theory and Application of Fault-Related Folding in Foreland Basins, Beijing, China. PetroChina Ltd and Princeton University, 43–44.
- [27] Law, B.E., R.M. Pollastro., and C.W. Keighini.: 1986. Geologic characterization of low permeability gas reservoirs in selected wells, greater green river basin, Wyoming, Colorado and Utah, in C.Spencer and R.Mast, eds., *geology of tight gas reservoirs* ; AAPG Studies in geology; vol.29;pp.253-269.
- [28] Morgan, R. 2003. Prospectivity in ultradeep water: the case for petroleum generation and migration within the outer parts of the Niger Delta apron. In: Arthur, T.J., McGregor, D.S. & Cameron, N.R. (eds) *Petroleum Geology of Africa: new themes and developing technologies*. Geological Society, London, Special Publications, 207, 151–164. <https://doi.org/10.1144/GSL.SP.2003.207.8>.
- [29] NFOR, Bruno Ndichoet al., (2011). Porosity as an overpressure zone indicator in an X-field of The Niger Delta Basin, Nigeria Arch. Appl. Sci. Res., 2011, 3 (3):29-36.
- [30] Nwaufa, W.A., Horsfall, D.E., and Ojo, C.A.: 2005. Advances in deep drilling in the Niger delta, 1970-2005: NAOC Experience, NAPE Conference Proceedings, August 2006, pp.5- 14.
- [31] Olatunbosunetal., (2014). Detecting and Predicting Over Pressure Zones in the Niger Delta, Nigeria: A Case Study of Afam Field. *Journal of Environment and Earth Science* ISSN 2224-3216 (Paper) ISSN 2225-0948 (Online). Vol. 4, No.6, 2014.
- [32] Oilfield review, 2005.
- [33] Reda, M. A., Ghorab, M. A., and Shazly, T. F. (2003). Determination of permeability and density and nature of fluids of some Miocene-Pre Miocene rocks in the central Gulf of Suez. *Egypt. J. Appl. Geophys.* 2:129–138.
- [34] Said, R. (1990). *The geology of Egypt*. Rotterdam, the Netherlands: Brookfield.
- [35] Schieber, J., Zimmerle, W., and Scthi, P. (1998). *Shale and mudstone* (Vols. 1 and 2). Stuttgart, Germany: Schweizerbart'scheVerlag
- [36] Schlumberger. (1986). *Repeat Formation Tester*. Princeton Junction, NJ:
- [37] Shaker, S., 2007, Calibration of Geopressure Predictions using the Normal Compaction Trend: Perception and Pitfall: CSEG Recorder, 7 p.
- [38] Shaker, S. S. 2012: Drilling Challenges due to the disparity between reservoir and seal pressure gradient: Based on a case Histories from Gulf of Mexico, American Association of Drilling Engineers AADE-12-FTCE-66.
- [39] Shaker, S. S., 2007, the precision of normal compaction trend delineation is the key stone of predicting pore pressure. AADE-07-NTCE-51.
- [40] Swarbrick, R.E., Osborne, M.J. & Yardley, G.S. 2002. Comparison of overpressure magnitude resulting from the main generating mechanisms. In: Huffman, A.R. & Bowers, G.L. (eds) *Pressure regimes in sedimentary basins and their prediction*. American Association of Petroleum Geologists Memoir, 76, 1–12.
- [41] Swarbrick, R.E. 2002, Challenges of Porosity-based Pore Pressure Prediction: CSEG Recorder, 4 p.
- [42] Ward, C.: 1995. Evidence for sediment unloading caused by fluid expansion overpressure generating mechanisms, in M. Fejerskov, and A.M. Myrvang, eds., *Proceedings of the Workshop on Rock Stress in the North Sea*; Trondheim, Norway, SINTEF and the University of Trondheim, 13 – 14 February; pp.218 –231.
- [43] Workshop Module, 2007, Pore Pressure Prediction and Wellbore Stability Workshop: Knowledge System, Nov 7th-8th, 2007.
- [44] Yoshida, C., et al.: "An Investigative Study of Recent Technologies Used for Prediction, Detection, and Evaluation of Abnormal Formation Pressure and Fracture Pressure in North and South America," IADC/SPE 36381 presented at the 1996 IADC/SPE Asia Pacific Drilling Technology Conference, Kuala Lumpur, Malaysia, September 9 – 11. <https://doi.org/10.2118/36381-MS>.